ERJ
Engineering Research Journal
Faculty of Engineering
Minoufiya University

STUDY OF TURBULENT FLOW IN RECTANGULAR CHANNEL WITH INCLINED BAFFLES

M. Nasr mostafanasr@yahoo.com
A. Abdel- Fattah ashourabdelfatah@yahoo.com
W. A. El-Askary wageeh_elaskary@yahoo.com
Mechanical Power Engineering Department, Faculty of Engineering, Menoufiya University, Shebin El-Kom, EGYPT

ABSTRACT

Experimental and numerical studies investigate the pressure recovery coefficient along the wall of a rectangular channel fitted by inclined-perforated and solid baffles. Two baffles of same overall size are used in the experiment. The upstream baffle is attached to the top surface, while the position, orientation, and the shape of the other baffle are varied. Different inflow Reynolds number for this study is tested and ranged between 71,000 and 122,500. Experimental results show that the pressure recovery distribution is strongly depended on the position, orientation, and geometry of the second baffle plate. The pressure drop goes down with an increase in the Reynolds number, but its value depends on the arrangement of baffles. The pressure drop is much higher for two inclined baffles (one perforated on the upper wall and one solid on the lower wall). For the sake of numerical simulation, the turbulent governing equations are solved by a control volume-based finite difference method and using the standard as well as the RNG $k-\varepsilon$ turbulence model associated with wall function to describe the turbulent structure. A modification including the effect of streamline curvature is considered in the turbulence model. The velocity and pressure terms of momentum equations are solved by SIMPLE (semi-implicit method for pressure-linked equation) method. Satisfied comparisons are achieved to verify the turbulence model used. The results show that the wall pressure recovery coefficient is strongly affected by the geometry and location of baffles in the duct. Also, the comparisons of the numerical results given by using turbulence models indicate the quality of the $k-\varepsilon$ including the streamline curvature in the turbulence model.

البحث يشمل دراسة عملية و نظرية لمعامل إسترجاع الضغط علي طول جدار لمجرى ذات مقطع مستطيل و مثبت داخلة عوائق صلبة مثقبة أو مصمتة و تميل بزاوية ثابتة علي جدار المجرى. العائق الأول مثبت بالسطح العلوى للمجرى بينما يتغير شكل و مكان و ترتيب العائق الثانى. تمت الدراسه فى ظروف سريان مختلفه فى رقم الرينولدز (من ٧١٠٠٠ إلى ١٢٢٥٠٠) عند الدخول. أظهرت النتائج المعمليه أن معامل إسترجاع الضغط يتأثر تأثر شديد بمكان و ترتيب و شكل العائق الثانى. و لقد اتضح أن الفقد فى الضغط ينخفض بزيادة رقم رينولدز فى حين تتأثر قيمته على حسب ترتيب العائق الثانى. و أظهرت النتائج أيضاً أن الفقد فى الضغط يكون كبير فى حالة استخدام عائقين العائق الأول مثقب على السطح العلوى و العائق الثانى مصمت على السطح السفلى.

تمت محاكاة النتائج العملية باستخدام نماذج عددية مختلفة يتم تطبيقها خلال نماذج (Standard k-ε)، (RNG k-ε) ، و كذالك نموذج (k-ε) المحسن بالأخذ فى الأعتبار تقوس خطوط الأنسياب. أظهرت مقارنة النتائج النظريه بالعملية توافق فى الأداء فى الحالات التى تمت دراستها بأستخدام النماذج العددية ، و لقد أظهرت النتائج مدى تحسن أداء النموذج (k-ε) المحسن بالأخذ فى الأعتبار تقوس خطوط الأنسياب. و هذا التطبيق يساعد فى فهم طبيعة السريان فى المجارى فى حالة و جود عوائق بأشكال مختلفة.

Keywords: Rectangular channel flow; Baffle; Inclined baffle; Pressure drop

1. INTRODUCTION

The use of baffled type channels is one of the commonly used passive heat transfer enhancement strategies in single-phase internal flow. This passive heat-transfer enhancement strategy has been used for various types of industrial applications such as heat exchanger, furnace design, nuclear reactor electronic cooling devices, thermal regenerators, internal cooling system of gas turbine blades and turbomachines.

Repeated ribs or turbulators have been used as the promoters of turbulence to enhance the heat transfer to the flow of coolants in a channel. These roughness elements break the laminar sub-layer of the flow. The heat transfer is enhanced as well as the pressure drop, an important parameter in the analysis of the overall performance of such flows. Investigations have been conducted to predict the effect of the number of ribbed walls on heat transfer and friction characteristics. Rib turbulators are widely used in gas

turbine cooling. These turbulators are installed on the two opposite sides of the cooling channel. In some cases, rib turbulators are casted on one side or four sides of the cooling channel. In spite of turbine blade internal cooling has been widely considered in the past studies, there are other applications such as heat exchangers, electronic equipment and nuclear reactors and may use the results of enhanced internal cooling in channels with one, two or four rib-roughened walls

Like jet impingement, ribs, and other heat transfer enhancement techniques, insertion of baffles in heat transfer devices is popular to promote better mixing of the coolant and increase cooling performance [1]. Applications of the inclined baffles may be in the large land based modern gas turbines, in which it has become a growing trend to increase the temperature of the combustion product to increase the specific thrust and to reduce the specific fuel consumption. Such a high temperature is far above the allowable temperature of super alloys and thermal barrier coatings (TBC) used in gas turbine blades. In gas turbine, usually air is used in the interior side of the blade to maintain the blade at the proper working temperature. Also in a number of other engineering and industrial applications such as, air-cooled solar collectors, laser curtain seals, labyrinth shaft seals, compact heat exchangers, and microelectronics, air is preferred as a coolant for its lightweight. However, due to the very low thermal conductivity internal cooling with gases is less effective than cooling with liquids. There are several techniques available to enhance the heat transfer coefficient of gases in internal cooling. The most commonly used technique for internal cooling enhancement is the placement of periodic ribs. Ribs are generally mounted on the heat transfer surface, which disturbs the boundary layer growth and enhances the heat transfer between the surface and the fluid. These ribs are small and do not disturb the core flow and therefore, the turbulence enhancement and boundary layer break down are mostly localized near the heat transfer surface. Ribs provide excellent cooling enhancement with a comparatively low penalty in the pressure drop increase for moderate Reynolds numbers, see Dutta and Dutta [1].

Impingement cooling as a second method uses high velocity jets to cool the surface of interest. However, often a large region needs to be cooled and multiple jets are required. Multiple jets get deflected in the presence of cross flow developed by upstream spent-jets.

The third one is a common internal cooling enhancement technique in which the placement of internal flow swirls, tape twisters, or baffles is used. The swirl insert and tape twister techniques create a significant amount of bulk flow disturbance, and the pressure drop penalties are much higher compared to the gain in heat transfer coefficient. Inclined solid baffles may be considered as a combination of ribs and channel inserts. The baffles are big enough to disturb the core flow, but like ribs, they are mounted on or near the heat transfer surface and can be periodic in nature. Perforations in inclined baffles create a multiple jet impingement condition and thus create a situation where all three major heat transfer coefficient enhancement techniques work in unison. Baffles also create bulk flow disturbance, but unlike tapes or swirls, baffles are discrete objects. Therefore, the flow disturbance created by baffles may be localized, but more intense. Usually the baffle plate is attached to the thermally active surface to augment heat transfer by providing additional fin-like surface area for heat transfer and better mixing [1].

In the past, experimental results were published with baffle plates perpendicular to the flow direction. Among important studies, Berner et al. [2] obtained mean velocity and turbulence results in flow over baffles; and Habib et al. [3] investigated heat transfer and flow over perpendicular baffles of different heights. But these works mainly emphasized on baffles that were perpendicular to the flow direction and for that reason penalties (friction factor) were higher than the improvements (heat transfer augmentation). However, it is possible to obtain enhanced heat transfer with comparably less frictional head loss by inserting inclined baffles in the flow path. These baffles are big enough to disturb the core flow, but like ribs, they are mounted on or near the heat transfer surface. Moreover, inclined perforated baffles contain circular holes, which facilitate jet impingement toward the heat transfer surface. Hence by utilizing inclined perforated baffles, the three major heat transfer augmentation techniques can be combined for effective cooling.

Dutta and Dutta [1] reported the enhancement of heat transfer with inclined solid and perforated baffles. In that study, the effects of baffle size, position, and orientation were studied for internal cooling heat transfer augmentation. Later on, a number of research groups have utilized the perforated baffle concept for internal cooling augmentation both experimentally (Ko and Anand [4]; Ziolkowska et al. [5]) and numerically (Yang and Hwang [6]; Yilmaz [7]; Tsay et al. [8]). In those studies, different aspect ratio channels and different porosity baffles were used; see Dutta and Hossain [9].

Several publications have addressed the state of the art review of turbine blade cooling and the analysis of flow with two opposite ribbed walls. The effects of flow Reynolds number and rib geometry (rib height, rib spacing, rib angle-of-attack, and rib configuration) on heat transfer and pressure drop in

the fully developed region of uniformly heated square channels have been investigated [10, 11]. Further study of the combined effects of rib geometry and channel aspect ratio on the local values of heat transfer and pressure drop was also reported [12–14]. The results show that the angled ribs provide a better heat transfer performance than transverse ribs, and the lower aspect ratio (AR) channels perform better than the higher aspect ratio channels.

The heat/mass transfer analogy has been applied to study detailed heat transfer distribution in two-pass and three-pass rectangular channels [15–19]. The square channel with parallel and crossed arrays of cross cut and beveled discrete ribs has been studied [20, 21]. Also, the effect of the equally segmented ribs arranged in both aligned and staggered arrays on two opposite walls of a square channel has been reported [22].

A paper presenting results of an experimental study of heat transfer and friction in rectangular ducts with baffles (solid or perforated) attached to one of the broad walls was published by Karwa et al. [23]. They used boundary conditions correspond closely to those found in solar air heaters. The friction factor for the solid baffles is found to be 9.6–11.1 times of the smooth duct. Performance comparison with the smooth duct at equal pumping power shows that the baffles with the highest open area ratio give the best performance.

Recently, experimental study attempted to explore the local heat transfer in rectangular channel with baffles was carried out by Lin [24]. Lin [24] analyzed the experimental results of baffles with different heights and bores in the event of different Reynolds numbers and heating quantities. He found that; apart from increasing the perturbation of flow field, the channel's flow field with baffles, which is similar to a backward-facing step flow field, is very helpful to heat transfer.

In a more recent publication, a detailed study was conducted for different height of entry channel to uniformly heated rectangular channel with two different angles turned flow, and with one wall mounted baffle [25]. Kurtbas [25] concluded that the pressure drop and heat transfer rate are strongly increased with the presence of a baffle and turned flow compared with a straight duct.

In the present work experimental and numerical studies of pressure recovery behavior of isothermal-turbulent flow in a rectangular channel is presented for different configuration, positions, and orientations of inclined baffles attached to the upper and lower surfaces. The study also includes the effect of the inflow Reynolds number on the pressure recovery.

2. EXPERIMENTAL SETUP

The experiments were conducted in the heat engine laboratory of the Faculty of Engineering, Menoufiya University. Figure 1 (a) shows a simple schematic view of the experimental setup. Filtered air to the test facility was supplied from two-parallel connected screw compressors. The maximum delivery pressure from the compressors is 15 bar. Each of the two compressors is capable of delivering $0.054 m^3/s$ compressed air to a large air reservoir from which the air passes through a control valve in the main pipeline of $10cm$ diameter. Therefore, the inflow discharge to the working section is manually regulated. A settling pipe of 4 hydraulic-diameter length is installed followed by a duct converter, smoothly converting the circular cross-section to a rectangular cross-section duct of the working section; see El-Askary and Nasr [26]. The test section used in the present paper is manufactured from steel. Its cross-sectional area is $W \times H = 12cm \times 5cm$ (internal dimensions) and length 100 cm.

Both (steel) solid and perforated baffles are of the same overall size (length L=29 cm, width W=12 cm and thickness t=3 mm) and utilized in the present study. The schematic view of the perforated baffles is given in Fig. 1 (b). The leading edges of the baffles are kept sharp to reduce the flow disturbance by the protruding edge. All perforated baffles have uniform holes of diameter $d = 1cm$. A total of three baffles, two perforated baffles and one solid are used. The summary of these baffles dimensions is presented in Table (1). In all arrangement, constant inclination angle of five degrees is maintained constant for both plates. This small inclination angle keeps these plates streamlined with the flow, and hence they avoid major flow blockage [9].

The experimental work was done through two cases. The first case is done without baffles. The second case is done with different baffle arrangements, see Table 1.

The experimental study was only aimed to measure the static wall-pressure distributions along the lower wall of the duct. The wall static pressure was measured through 1 *mm* diam. pressure taps on the wall along the center plane of duct. The uncertainties in measuring wall pressure led to an uncertainty in the wall static pressure coefficient of ± 0.009. The measurements of the static pressure distribution were conducted using multi-tube water manometer. The inflow Reynolds number was determined from the measured flow rate (Q) through a calibrated orifice meter fitted with a mercury U-tube manometer with an accuracy of 1.5 %.

The wall pressure distributions are sampled in the form of wall pressure recovery coefficient defined as

$C_p = \frac{\bar{p} - \bar{p}_{ref}}{0.5\rho U_{in}^2}$, where $\bar{p}_{ref}$ is the atmospheric pressure and $U_{in} = \frac{Q}{W \times H}$ is the average velocity at entrance [26].

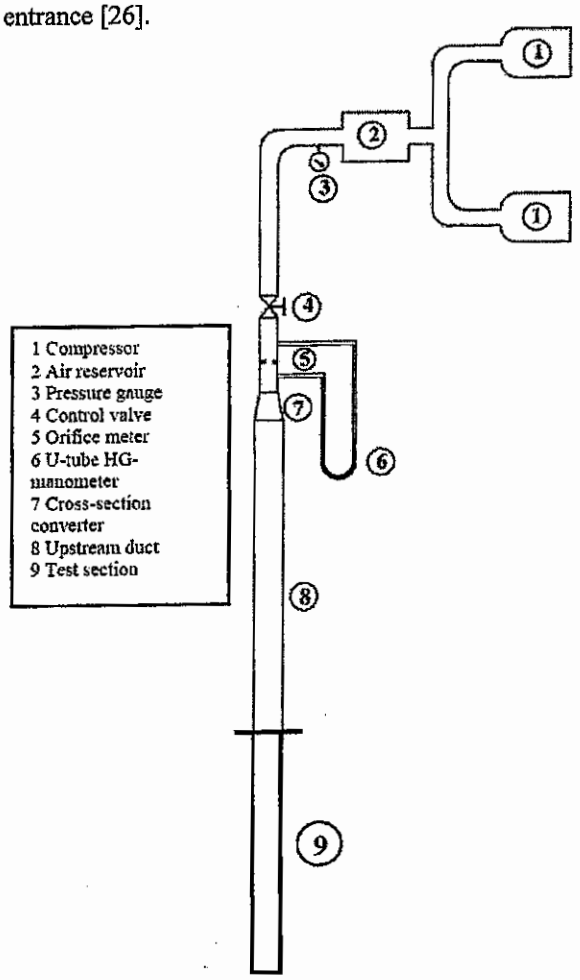

Fig. 1.a Schematic diagram of the experimental setup

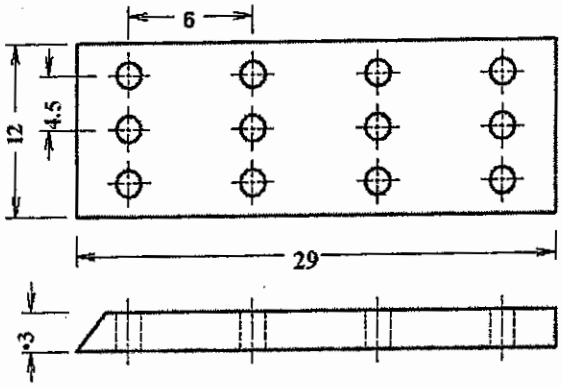

Fig. 1.b a perforated baffle plate (dimensions in cm.)

Table 1 Different baffle configurations used in the experiments, see Fig. (2)

Case study	*C (cm)*	*Baffles*	*Attachment of Baffle to surfaces*	*Fixed dimensions (cm)*
1	29	1 perforated and 1 solid	one perforated up and one solid down	A=1.25, B=2.5
2	44.5	1 perforated and 1 solid	one perforated up and one solid down	A=1.25, B=2.5
3	60	1 perforated and 1 solid	one perforated up and one solid down	A=1.25, B=2.5
4	29	2 perforated	one on the top surface and the other on the down surface	A=1.25, B=2.5
5	44.5	2 perforated	one on the top surface and the other on the down surface	A=1.25 ,B=2.5
6	60	2 perforated	one on the top surface and the other on the down surface	A=1.25, B=2.5
7	29	2 perforated	Top surface	A=1.25, B=2.5
8	44.5	2 perforated	Top surface	A=1.25, B=2.5
9	60	2 perforated	Top surface	A=1.25, B=2.5

3. MATHEMATICAL MODEL

The physical model used in this study is shown in Figure 2, where two-dimensional incompressible-turbulent flow is considered. In the present study, it is assumed that the fluid (air) is incompressible and Newtonian with temperature-independent fluid properties.

Based on the characteristics scales of H (the duct cross-section height) and U_{in} (the inflow bulk velocity), the dimensionless variables are defined as follows: $x = \frac{\bar{x}}{H}$, $y = \frac{\bar{y}}{H}$, $k = \frac{\bar{k}}{U_{in}^2}$, $u = \frac{\bar{u}}{U_{in}}$, $v = \frac{\bar{v}}{U_{in}}$, $p = \frac{\bar{p}}{0.5\rho U_{in}^2}$, $\varepsilon = \frac{\bar{\varepsilon} H}{U_{in}^3}$, where, the over bar represents the dimensional quantities. According to the above assumptions and dimensionless variables, the dimensionless governing equations are expressed as the following:

Continuity equation:

$$\frac{\partial u}{\partial x}+\frac{\partial \mathrm{v}}{\partial y}=0 \tag{1}$$

Momentum equations:

$$u\frac{\partial u}{\partial x}+\mathrm{v}\frac{\partial u}{\partial y}=-\frac{\partial p}{\partial x}+\frac{\partial}{\partial x}\left[\left(\frac{1}{\mathrm{Re}}+\frac{1}{\mathrm{Re}_t}\right)\frac{\partial u}{\partial x}\right]+\frac{\partial}{\partial y}\left[\left(\frac{1}{\mathrm{Re}}+\frac{1}{\mathrm{Re}_t}\right)\frac{\partial u}{\partial y}\right]+\frac{\partial}{\partial x}\left(\frac{1}{\mathrm{Re}_t}\frac{\partial u}{\partial x}\right)+\frac{\partial}{\partial x}\left(\frac{1}{\mathrm{Re}_t}\frac{\partial v}{\partial y}\right) \tag{2}$$

$$u\frac{\partial \mathrm{v}}{\partial x}+\mathrm{v}\frac{\partial \mathrm{v}}{\partial y}=-\frac{\partial p}{\partial y}+\frac{\partial}{\partial x}\left[\left(\frac{1}{\mathrm{Re}}+\frac{1}{\mathrm{Re}_t}\right)\frac{\partial \mathrm{v}}{\partial x}\right]+\frac{\partial}{\partial y}\left[\left(\frac{1}{\mathrm{Re}}+\frac{1}{\mathrm{Re}_t}\right)\frac{\partial \mathrm{v}}{\partial y}\right]+\frac{\partial}{\partial x}\left(\frac{1}{\mathrm{Re}_t}\frac{\partial u}{\partial y}\right)+\frac{\partial}{\partial y}\left(\frac{1}{\mathrm{Re}_t}\frac{\partial \mathrm{v}}{\partial y}\right) \tag{3}$$

The dimensionless equations for standard k- ε model are written as:

$$u\frac{\partial k}{\partial x}+\mathrm{v}\frac{\partial k}{\partial y}=\frac{\partial}{\partial x}\left[\left(\frac{1}{\mathrm{Re}}+\frac{1}{\sigma_k\,\mathrm{Re}_t}\right)\frac{\partial k}{\partial x}\right]+\frac{\partial}{\partial y}\left[\left(\frac{1}{\mathrm{Re}}+\frac{1}{\sigma_k\,\mathrm{Re}_t}\right)\frac{\partial k}{\partial y}\right]+G-\varepsilon \tag{4}$$

$$u\frac{\partial \varepsilon}{\partial x}+\mathrm{v}\frac{\partial \varepsilon}{\partial y}=\frac{\partial}{\partial x}\left[\left(\frac{1}{\mathrm{Re}}+\frac{1}{\sigma_\varepsilon\,\mathrm{Re}_t}\right)\frac{\partial \varepsilon}{\partial x}\right]+\frac{\partial}{\partial y}\left[\left(\frac{1}{\mathrm{Re}}+\frac{1}{\sigma_\varepsilon\,\mathrm{Re}_t}\right)\frac{\partial \varepsilon}{\partial y}\right]+c_1\frac{\varepsilon}{k}G-c_2\frac{\varepsilon^2}{k} \tag{5}$$

Where G is the rate of production of turbulent kinetic energy and is given by:

$$G=\frac{2\,S^2}{\mathrm{Re}_t} \tag{6}$$

and

$$S^2=\frac{1}{2}\left[\left(\frac{\partial \mathrm{v}}{\partial x}+\frac{\partial u}{\partial y}\right)^2+2\left(\frac{\partial u}{\partial x}\right)^2+2\left(\frac{\partial \mathrm{v}}{\partial y}\right)^2\right] \tag{7}$$

The empirical values of the model constants are reported as: c_1=1.44 , c_2 = 1.92, c_μ =0.09, σ_k= 1 and σ_ε=1.3.

Leschziner and Rodi [27] incorporated the effects of streamline curvature on c_μ in the form

$$c_\mu = Max\left\{0.025,\frac{0.09}{\left[1+0.57\frac{k^2}{\varepsilon^2}\left(\frac{\partial V_{tot}}{\partial n}+\frac{V_{tot}}{R_c}\right)\frac{V_{tot}}{R_c}\right]}\right\} \tag{8}$$

Where, $V_{tot}=\sqrt{u^2+v^2}$ is the total velocity.

The curvature radius is

$$\frac{1}{R_c}=\frac{uv\left(\frac{\partial u}{\partial x}-\frac{\partial \mathrm{v}}{\partial y}\right)+\mathrm{v}^2\frac{\partial u}{\partial y}-u^2\frac{\partial \mathrm{v}}{\partial x}}{\left(u^2+\mathrm{v}^2\right)^{1.5}} \tag{9}$$

The dimensionless form of dissipation rate for renormalization group model (RNG model) is written as [28]:

$$u\frac{\partial \varepsilon}{\partial x}+v\frac{\partial \varepsilon}{\partial y}=\frac{\partial}{\partial x}\left[\left(\frac{1}{\mathrm{Re}}+\frac{1}{\sigma_\varepsilon\,\mathrm{Re}_t}\right)\frac{\partial \varepsilon}{\partial x}\right]+\frac{\partial}{\partial y}\left[\left(\frac{1}{\mathrm{Re}}+\frac{1}{\sigma_\varepsilon\,\mathrm{Re}_t}\right)\frac{\partial \varepsilon}{\partial y}\right]+\frac{\varepsilon}{k}\left(c_1-\frac{\eta\left(1-\frac{\eta}{\eta_0}\right)}{1+\beta\eta^3}\right)G-c_2\frac{\varepsilon^2}{k} \tag{10}$$

where $\eta=\sqrt{c_\mu^{-1}\frac{G}{\rho\varepsilon}}$.

The values of the model constants are taken as:
$c_\mu=0.085, c_1=1.44, c_2=1.68, \sigma_k=1.39, \sigma_\varepsilon=1.39,$
$\eta_0=4.38$ *and* $\beta=0.012$

The eddy viscosity μ_t is given by the relation

$$\mu_t=c_\mu\frac{\rho\,k^2}{\varepsilon} \tag{11}$$

The boundary conditions for the above set of governing equations are as follows:

a) Inlet boundary

The uniform velocity profiles and turbulent kinetic energy and its dissipation rate are imposed at the inlet boundary, *i.e.*, $\bar{u}_i=U_{in}$, $\bar{k}_i=0.01\,U_{in}^2$ and $\bar{\varepsilon}_i=\frac{c_\mu\bar{k}_i^{1.5}}{0.1H}$.

b) Wall boundary

At the wall, the no slip boundary condition is imposed, $\bar{u}=\bar{\mathrm{v}}=0$ and using the wall function suggested by Launder and Spalding [29] to compute the near wall velocity. The law of the wall is used to

modify the flow parameters $\bar{u}, \bar{v}, \bar{k}$ *and* $\bar{\varepsilon}$ at the nearest grid point.

In the porous region, the contribution of turbulence in a porous region is neglected by setting the turbulent contribution to viscosity equal to zero. In addition, the generation of turbulence will be set to zero in the medium.

c) Exit boundary

A zero gradient condition is employed for the outlet boundary. Although this boundary condition is strictly valid only when the flow is fully developed, it is also permissible for sufficient downstream from the region of interest, i.e., $\frac{\partial \phi}{\partial x} = 0$ and $\phi = \bar{u} = \bar{v} = \bar{k}$ *and* $\bar{\varepsilon}$

4. SOLUTION PROCEDURE

The mathematical models described above consist of a set of differential equations subject to appropriate boundary conditions. To provide the algebraic form of the governing equations, a fully staggered grid system is adopted for the velocity components and the scalar variables. These equations are discretized using a control volume finite difference method (CVFDM). The numerical solution in the present work is accomplished using Semi- Implicit Method for Pressure Linked Equation (SIMPLE) utilized by Patankar [30]. The velocity component u is calculated at the east and west faces of the main control volumes from the solution of the axial momentum equation. Similarly, the velocity component v at the north and south faces is calculated. When the pressure correction equation is solved, then the velocities and the pressure fields are corrected. To complete iteration, the turbulent kinetic energy and energy dissipation rate are solved successively. The discretization equations are solved by the line by line procedure, which is a combination of Gauss- Seidel and tridiagonal matrix algorithm in the streamwise direction. The tridiagonal matrix algorithm (TDMA) is used to solve a set of discretization equations in the cross- stream direction. Relaxation factors are employed to promote smooth convergence of the discretized equations. The relaxation factors are controlled to be 0.75, 0.75, 0.5, 0.5, and 0.5 for u, v, p, k and ε, respectively. The turbulent viscosity is also under-relaxed at a value of 0.5. The converged criterion in this study is based on the successive changes in variables. All field variables are monitored, and the following condition is used to declare convergence:

$$MAX\left|\frac{\phi_{i,j}^{n} - \phi_{i,j}^{n-1}}{\phi_{i,j}^{n}}\right| \le 10^{-4} \qquad (12)$$

In addition, the ratio of the difference between the inlet mass flow rate and the outlet mass flow rate to the inlet mass flow rate is also examined. Convergence is declared if the relative mass imbalance is less than 10^{-3} and Equation (12) are satisfied simultaneously. To verify the algorithm, numerical tests are performed to ensure that the solution is grid algorithm.

The grid points are distributed uniformly over the computational domain. A 350×150 grid points are placed in the computational domain after different tests of grid dependence, see Fig.2 (d).

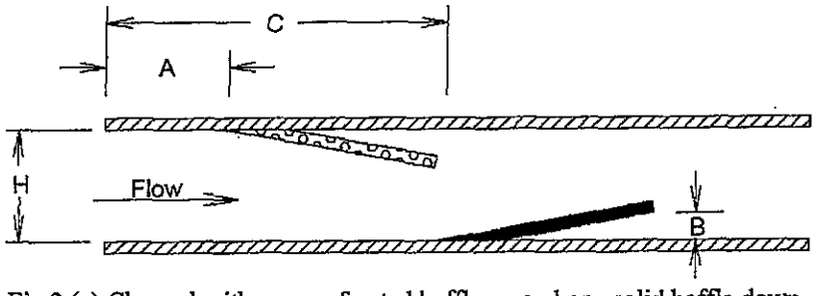

Fig.2 (a) Channel with one perforated baffle up and one solid baffle down

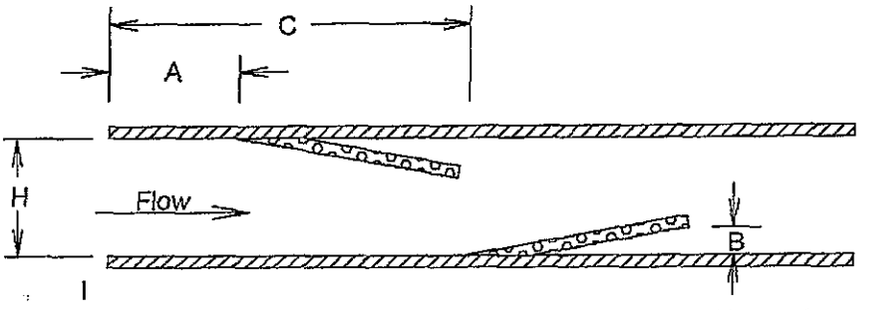

Fig.2 (b) Channel with one perforated baffle up and one perforated baffle down

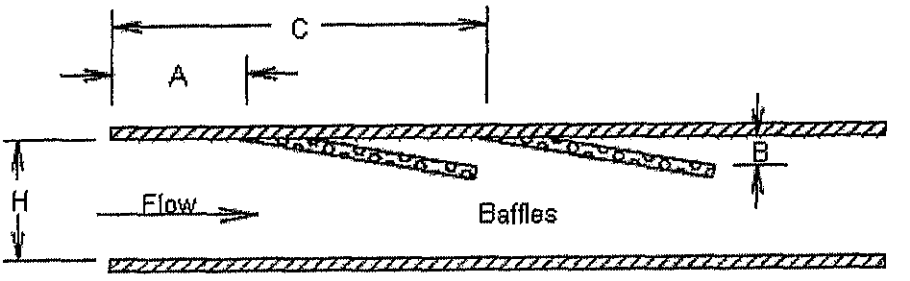

Fig. 2 (c) Channel with two perforated baffles on up wall

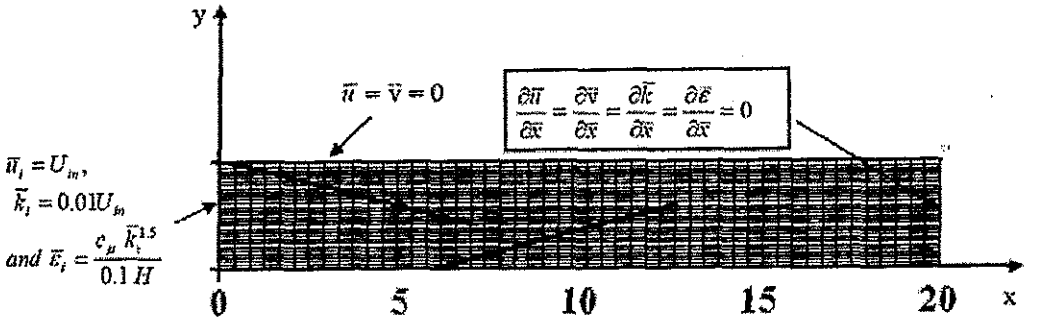

Fig. 2 (d) Grid generated to the channel with two inclined baffles

5. RESULTS AND DISCUSSION

The performance of the various discussed $k-\varepsilon$ models is first tested. The local pressure recovery coefficient Cp along the lower wall of the duct with the presence of one perforated baffle on the upper wall and another one on the lower wall (case 4, see Table 1) is presented in Fig. 3 for all tested turbulence models. As noticed the standard and the improved streamline curvature $k-\varepsilon$ models capture the shape of the pressure distribution. However, the improved $k-\varepsilon$ model of Leschziner and Rodi [27] adequately fits the experimental data, so it will be used for all other simulation cases.

Figure 4 shows the pressure coefficient on the bottom wall of a smooth channel without any installed baffles with dimensionless downstream distance x/H for different values of Reynolds number using k-ε model with correction of Leschziner and Rodi [27]. The trend of pressure generally decreases in the downstream direction. As Reynolds number increases, the pressure coefficient decreases due to the friction losses increasing.

Figure 5 represents the relation between the pressure recovery coefficient Cp and the dimensionless downstream distance x/H at bottom wall of the channel with two inclined baffles of 5° inclined angle. One baffle is perforated and located on the upper wall at dimensionless distance A/H =0.25 from the inlet of channel and a second baffle is solid and located on the bottom wall at different dimensionless distances, C/H=5.8, 8.9 and 12 from the inlet of channel (cases 1, 2 and 3, see Table 1). The plots show the effect of Reynolds number on the pressure recovery coefficient. Three different values of channel Reynolds number 71,000, 100,000 and 122,500 are considered, respectively. From Figure 5(a), it can be seen that the pressure decreases with downstream distance until the location of the second baffle. This is due to the acceleration of flow near the bottom wall with the downstream distance. It fills down suddenly behind the baffle to minimum value and then increases again reaching the reattachment point and it slowly increases to reach the atmospheric pressure at the duct exit. It may be expected to be an effect of a recirculation zone generated behind the baffle. Also from the Figure, it is seen that the pressure coefficient decreases by increasing Reynolds number. This is because the hydraulic losses are decreasing with increasing Reynolds number. The increment of the pressure recovery coefficient decreases in the front of the second baffle by changing its location in downstream direction C/H=8.9. When the location of second baffle is at C/H=12, the effect of the first baffle is appearances at the begging at x/H=6. The pressure in this zone decreases with downstream due to the hydraulic losses. But the pressure recovery coefficient increases after the second baffle and this may be due to the presence of the recirculation zone behind the second baffle, see Figure 5 (c).

Figure 6 shows the relation between the pressure recovery coefficient and the dimensionless downstream distance x/H at bottom wall of the channel with two inclined perforated baffles with the same inclined angle of 5 degrees. One perforated baffle is located on the upper wall at a distance

A/H=0.25 from the inlet and second perforated baffle is installed on the bottom wall at different dimensionless distances, C/H=5.8, 8.9 and 12 from the inlet of channel (cases 4, 5 and 6, see Table 1). From this Figure, it can be seen that the trend of the pressure recovery coefficient is same like that trend of the pressure in Figure 5, but with lower values of pressure. This is due to the flow leakages which pass through the holes in the second baffle in the form of jets which impinge the lower wall and hence causes an increase of pressure on the surface

Figure 7 indicates the relation between the pressure recovery coefficient and the dimensionless downstream distance x/H at bottom wall of the channel with the presence of two installed inclined perforated baffles with 5°-inclination angle. These perforated baffles are fixed on the up wall. The first perforated baffle is installed at a distance A/H=0.25 from the inlet and second perforated baffle installed in the upper wall also at various distances, C/H=5.8, 8.9 and 12 from the inlet of channel (cases 7, 8 and 9, see Table 1). From Fig. 7(a), it can be seen that the pressure recovery coefficient decreases to a first minimum value and then increases to a peak value. The location of this peak value appears to be in the space between the baffle plates. The pressure coefficient decreases again to second minimum value. It increases again to reach zero value at outlet section. The first minimum value of the pressure is due to the flow acceleration near the bottom side of channel at face of the first baffle edge. In this zone the velocity increases because the flow area becomes narrow, consequently the pressure becomes lower. The flow area increases between the two baffles then the velocity decreases in this zone accordingly the pressure increases. The flow area reduces again in downstream direction because of the second inclined perforated baffle, then the kinetic energy increases and it becomes high at the second baffle edge then the pressure becomes minimum value. After the second baffle edge, the flow area increases, consequently the velocity decreases and then the pressure recovery coefficient increases.

The effect of the second perforated baffle location on the pressure recovery is separately studied and included in Fig. 8. For different locations of the second inclined perforated baffle C/H= 5.8, 8.9 and 12 from the inlet of channel at constant Reynolds number Re = 71000, the experimental and numerical values are presented. This plot reveals that the value of pressure coefficient increases upstream of the second baffle. This is because the flow area increases as the second baffle shifts in downstream direction then the velocity decreases consequently the pressure increases. As the location of second baffle shifts toward downstream direction, the minimum value of the pressure decreases, which occurs in the recirculation zones behind the second baffle location. This is due to the disturbance of the flow in recirculation zone becomes strong causing an increase of the hydraulic losses.

The effect of the type of the second inclined baffle (i.e., perforated baffle or solid baffle) on the pressure recovery coefficient on the bottom wall at Re = 71000 is shown in Figure 9. From this Figure, it is seen that, in case of the channel without baffles, the pressure recovery coefficient decreases with downstream direction. The pressure increases in case of channel with baffles one perforated baffle on the upper wall and the second baffle on the bottom wall. This is because the existing of the baffles decelerates the flow and hence the pressure increases. In case, the second perforated baffle is installed, the pressure is less than the case of solid baffle. This is due to the leakage of the flow in the perforated baffle, and then the pressure reduces.

A representative selection of x-component velocity contours ($\overline{u}/U_{in}$) using the numerical results of k-ε model with correction of Leschziner and Rodi [27] for Re = 71000 and the location of first perforated baffle (A/H=0.25) and the second baffle at C/H = 5.8 with baffle angle (θ = 5°) is shown in Figure 10. From this Figure, it can be seen that the velocity concentrates in the gape between the two baffles and the flow passages from the holes as jets forms in the perforated baffle. Five recirculation zones generate behind the first perforated baffle. The same recirculation zones appear behind the second perforated baffle, see Fig. 10(a). But one recirculation zone appears behind the second solid baffle at same location as shown in Fig. 10(b). The length of this recirculation zone is bigger than the length of recirculation zone for the case of second perforated baffle. This is because the second solid baffle does not allow any flow jets and it deflects the entire flow toward the upper wall. When the second perforated baffle is fixed at the same location C/H=5.8 on the upper wall, the lengths of recirculation zones behind the first perforated baffle are decreased. This is due to the effect of second perforated baffle.

Figure 11 represents the effect of location of second perforated baffle on the x-component velocity contours ($\overline{u}/U_{in}$) using k-ε model with correction of Leschziner and Rodi [27]. From this Figure, it is noticed that the recirculation zones behind the first baffle increases by shifts the location of second baffle towards downstream direction. This is because the flow deflects quickly towards the upper wall with reduction of the dimensionless distance C/H of the second baffle location.

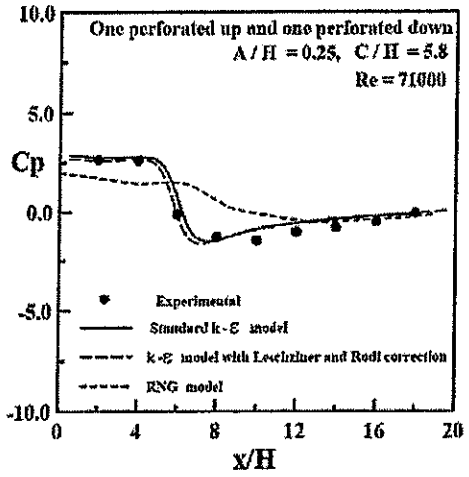

Fig. 3 Wall pressure coefficient on bottom wall of channel with different turbulence models

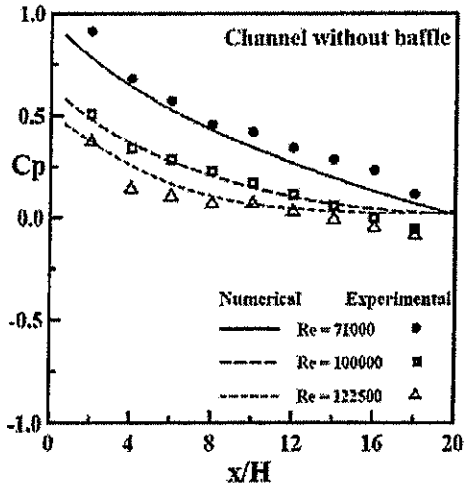

Fig. 4 Wall pressure coefficient on bottom wall of the channel at different Re using the k-ε with correction of Leschziner and Rodi [27]

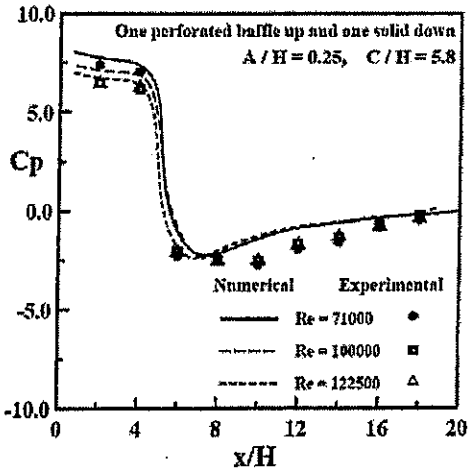

Fig. 5-a Second solid baffle on the bottom wall at C/H= 5.8

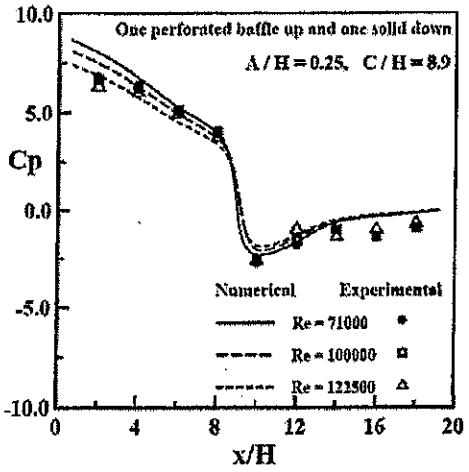

Fig. 5-b Second solid baffle on the bottom wall at C/H= 8.9

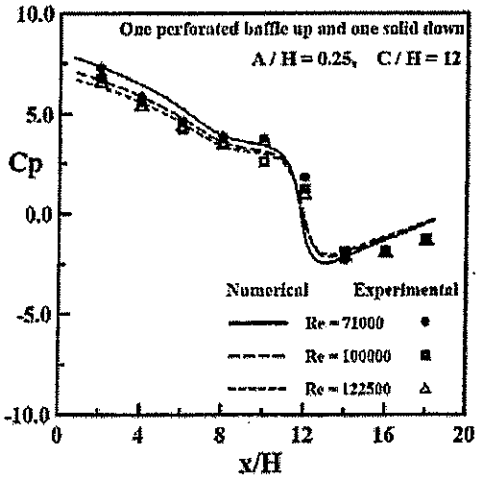

Fig. 5-c Second solid baffle on the bottom wall at C/H= 12

Fig. 5 Wall pressure coefficient on the bottom wall of channel for two baffles one perforated on up wall at A/ H = 0.25 at different value of Re using the k-ε with correction of Leschziner and Rodi [27]

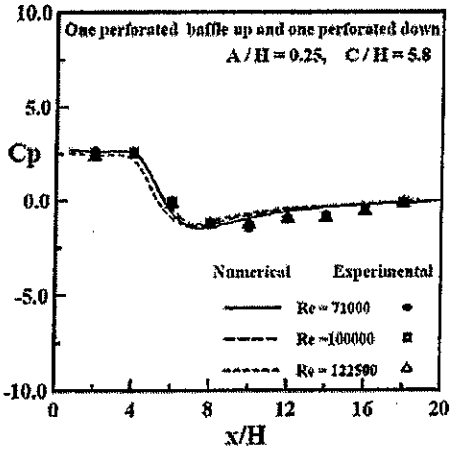

Fig. 6-a Second perforated baffle on the bottom wall at C/H= 5.8

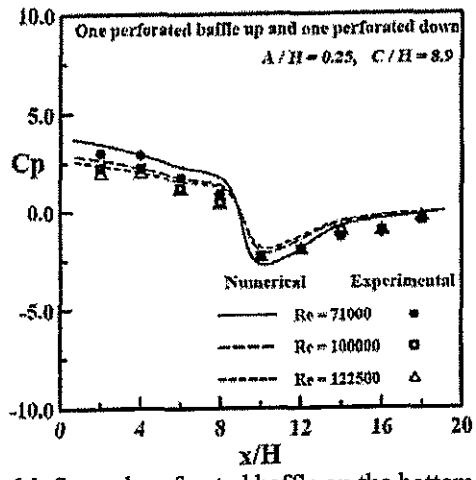

Fig. 6-b Second perforated baffle on the bottom wall at C/H= 8.9

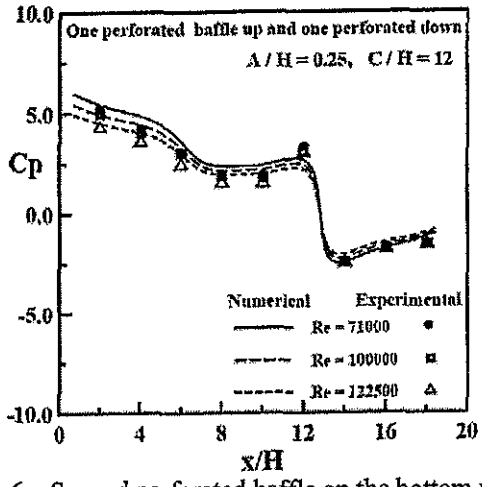

Fig. 6-c Second perforated baffle on the bottom wall at C/H= 12

Fig. 6 Wall pressure coefficient on the bottom wall of channel for two baffles one perforated on up wall at A/ H = 0.25 at different value of Re using the k-ε with correction of Leschziner and Rodi [27]

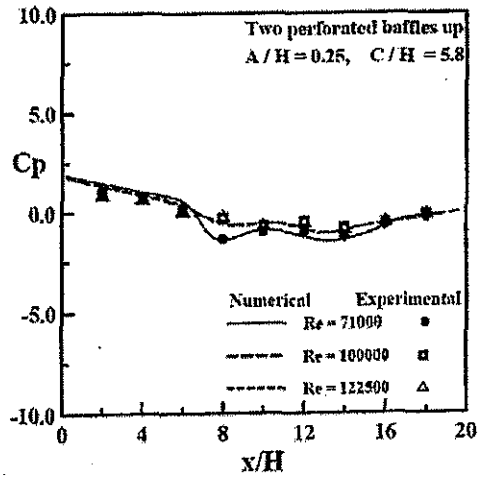

Fig. 7-a Second perforated baffle at C/H= 5.8

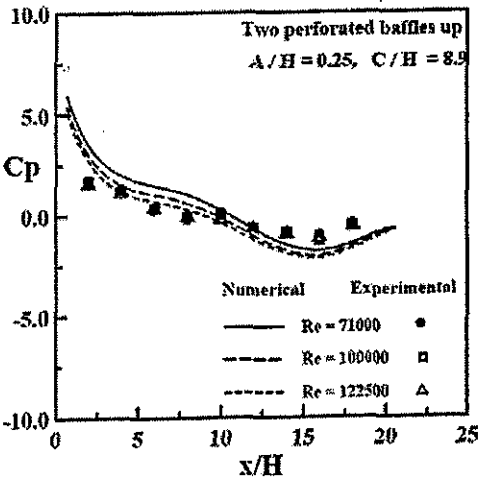

Fig. 7-b Second perforated baffle at C/H= 8.9

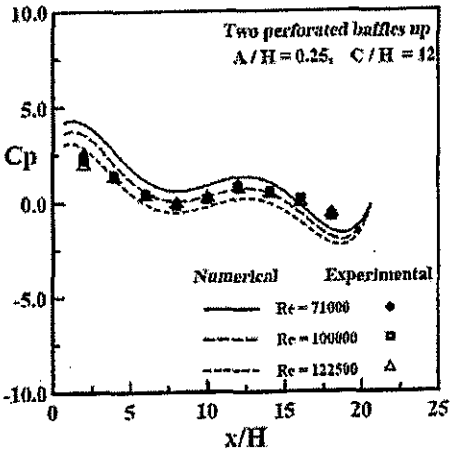

Fig. 7-c Second perforated baffle at C/H= 12

Fig. **7** Wall pressure coefficient on the bottom wall of channel for two baffles perforated on up wall at A/ H = 0.25 at different value of Re using the k-ε with correction of Leschziner and Rodi [27]

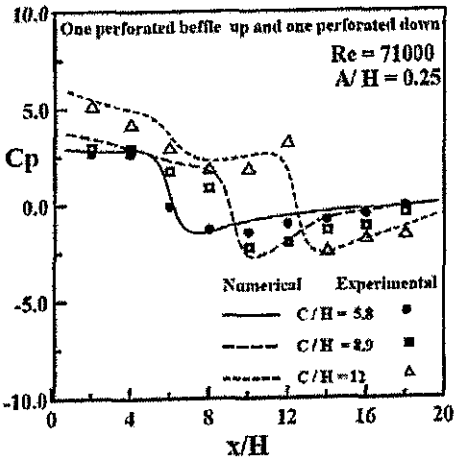

Fig. 8 Wall pressure coefficient on the bottom wall of channel with different location of second perforated baffle for two baffles at Re = 71000 using the k-ε with correction of [27]

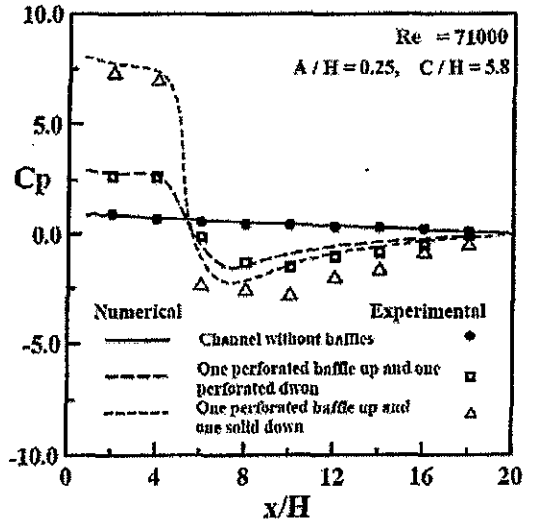

Fig. 9 Effect of baffles in channel on wall pressure coefficient on the bottom wall of channel using the k-ε at Re = 71000 with correction of [27]

6. CONCLUSIONS

In the present paper, experimental and numerical studies were performed to investigate the effect of inclined-perforated and solid baffles on the pressure recovery coefficient along the walls of a rectangular channel for different inflow velocities. The results showed that the pressure recovery distribution is strongly affected by the position, orientation, and geometry of the second baffle plate. The pressure drop goes down with an increase in the Reynolds number, but its value depends on the arrangement of baffles. The pressure drop is much higher for two inclined baffles (one perforated on the upper wall and one solid on the lower wall). The numerical simulation included different turbulence models; the standard $k-\varepsilon$, the modified $k-\varepsilon$ with including the streamline curvature and the RNG $k-\varepsilon$ turbulence models. Satisfied comparisons were achieved in better form from the modified $k-\varepsilon$.

This work will be experimentally and numerically extended to study the heat transfer from an upper heated wall with the presence of different shapes and orientation of baffles and different inflow conditions.

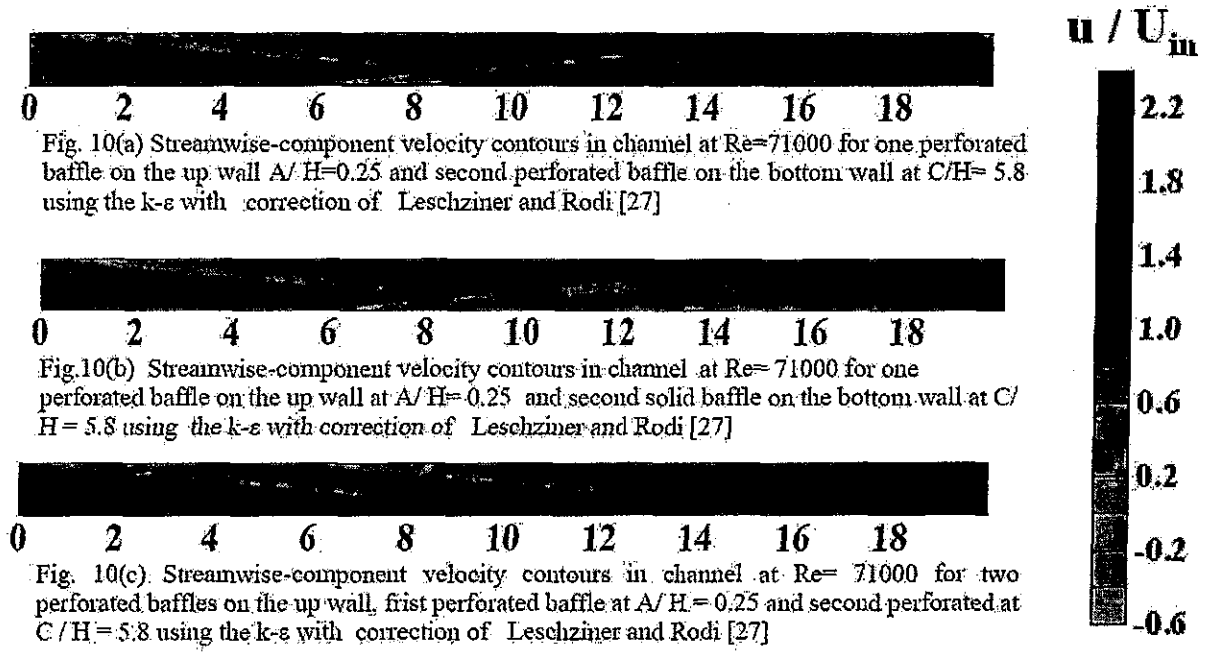

Fig. 10(a) Streamwise-component velocity contours in channel at Re=71000 for one perforated baffle on the up wall A/ H=0.25 and second perforated baffle on the bottom wall at C/H= 5.8 using the k-ε with correction of Leschziner and Rodi [27]

Fig.10(b) Streamwise-component velocity contours in channel at Re= 71000 for one perforated baffle on the up wall at A/ H= 0.25 and second solid baffle on the bottom wall at C/ H = 5.8 using the k-ε with correction of Leschziner and Rodi [27]

Fig. 10(c) Streamwise-component velocity contours in channel at Re= 71000 for two perforated baffles on the up wall, frist perforated baffle at A/ H = 0.25 and second perforated at C / H = 5.8 using the k-ε with correction of Leschziner and Rodi [27]

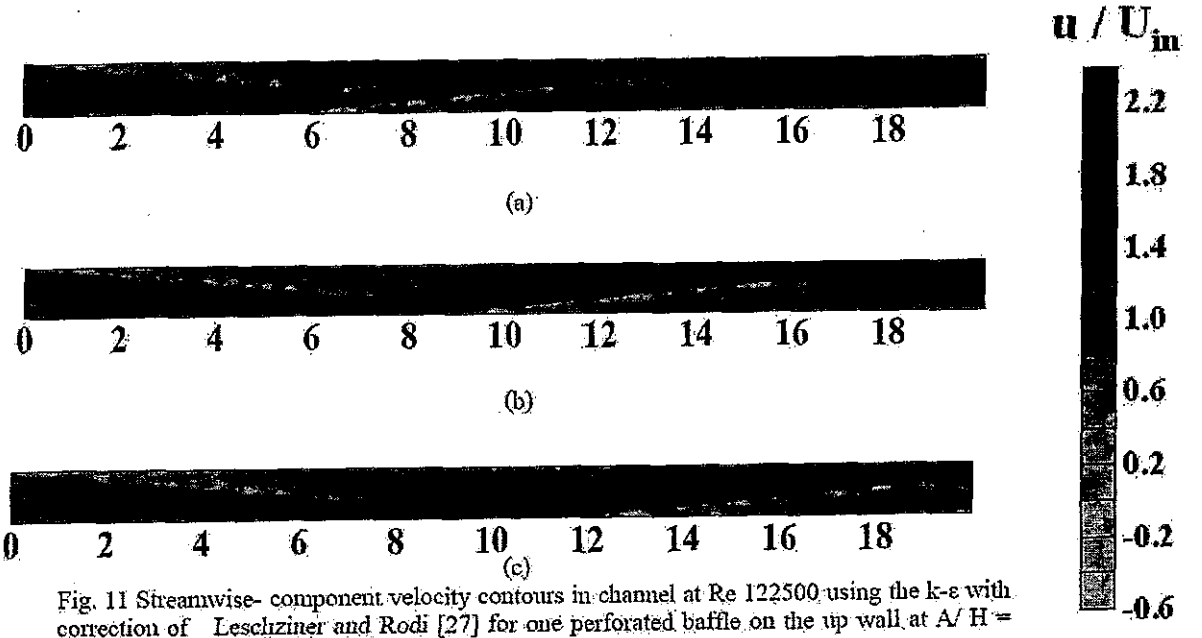

Fig. 11 Streamwise- component velocity contours in channel at Re 122500 using the k-ε with correction of Leschziner and Rodi [27] for one perforated baffle on the up wall at A/ H = 0.25 and second perorated baffle on the bottom wall.
(a) C / H = 5.8, (b) C/ H = 8.9 and (c) C/ H = 12

7. REFERENCES

[1] P. Dutta and S. Dutta, Effect of baffle size, perforation and orientation on internal heat transfer enhancement, *Int. J. Heat Mass Transfer* **41** (1998) (19), pp. 3005–3013.

[2] C. Berner, F. Durst and D.M. McEligot, Flow around baffles, ASME J. Heat Transfer 106 (1984), pp. 743-749.

[3] M.A. Habib, A.M. Mobarak, M.A. Sallak, E.A. Abdel Hadi and R.I. Affify, Experimental investigation of heat transfer and flow over baffles of different heights, *ASME J. Heat Transfer* **116** (1994) (2), pp. 363-368.

[4] K.H. Ko and N.K. Anand, Use of porous baffles to enhance heat transfer in a rectangular channel, *Int. J. Heat Mass Transfer* **46** (2003) (22), pp. 4191–4199.

[5] I. Ziolkowska, M. Dolata and D. Ziolkowski, Heat and momentum transfer in fluids heated in tubes with turbulence generators at moderate Prandtl and Reynolds numbers, *Int. J. Heat Mass Transfer* **42** (1999) (4), pp. 613–627.

[6] Y.T. Yang and C.Z. Hwang, Calculation of turbulent flow and heat transfer in a porous-baffled channel, *Int. J. Heat Mass Transfer* **46** (2003) (5), pp. 771–780.

[7] M. Yilmaz, The effect of inlet flow baffles on heat transfer, *Int. Commun. Heat Mass Transfer* **30** (2003) (8), pp. 1169–1178.

[8] Y.L. Tsay, J.C. Cheng and T.S. Chang, Enhancement of heat transfer from surface-mounted block heat sources in a duct with baffles, *Numer. Heat Transfer Part A* **43** (2003) (8), pp. 827–841.

[9] P. Dutta and A. Hossain, Internal cooling augmentation in rectangular channel using two inclined baffles, *Int. J. Heat Mass Transfer* **26** (2005), pp. 223–232.

[10] J.C. Han, Heat transfer and friction in channels with two opposite rib-roughened walls, J. Heat Transfer 106 (1984), pp. 774–781.

[11] J.C. Han, J.S. Park and C.K. Lei, Heat transfer enhancement in channels with turbulence promoters, J. Eng. Gas Turbines Powers 107 (1985), pp. 629–635.

[12] J.C. Han, Heat transfer and friction characteristics in rectangular channels with rib turbulators, J. Heat Transfer 110 (1988), pp. 321–328.

[13] J.C. Han and J.S. Park, Developing heat transfer in rectangular channels with rib turbulators, *Int. J. Heat Mass Transfer* **31** (1988), pp.183–195.

[14] J.C. Han, S. Ou, J.S. Park and C.K. Lei, Augmented heat transfer in rectangular channels of narrow aspect ratios with rib turbulators, *Int. J. Heat Mass Transfer* **32** (1989), pp. 1619–1630.

[15] J.C. Han, P.R. Chandra and S.C. Lau, Local heat/mass transfer distributions around sharp 180_ turns in two-pass smooth and rib-roughened channels, *Int. J. Heat Mass Transfer* **110** (1988), pp. 91–98.

[16] P.R. Chandra, J.C. Han and S.C. Lau, Effect of rib angle on local heat/mass transfer distribution in a two-pass rib roughened channel, J. Turbomachinery 110(1988), pp. 233–241.

[17] P.R. Chandra and J.C. Han, Pressure drop and mass transfer in two-pass ribbed channels, J. Thermophys. Heat Transfer 3 (1989), pp. 315–320.

[18] J.C. Han and P. Zhang, Pressure loss distribution in three-pass rectangular channels with rib turbulators, J. Turbomachinery 111 (1989), pp. 515–521.

[19] J.C. Han and P. Zhang, Effect of rib-angle orientation on local mass transfer distribution in a three-pass rib-roughened channel, J. Turbomachinery 113 (1991), pp.123–130.

[20] S.C. Lau, R.D. McMillin and J.C. Han, Turbulent heat transfer and friction in a square channel with discrete rib turbulators, J. Turbomachinery 113 (1991), pp. 360–366.

[21] S.C. Lau, R.D. McMillin and J.C. Han, Heat transfer characteristics of turbulent flow in a square channel with angled discrete ribs, J. Turbomachinery 113 (1991), pp. 367–374.

[22] R.T. Kukreja, S.C. Lau, R.D. McMillin and P.R. Chandra, Effects of length and configuration of transverse discrete ribs on heat transfer and friction for turbulent flow in a square channel, ASME/JSME Thermal Engineering Joint Conference 3, 213–218, Reno, Nevada, 1991.

[23] R. Karwa, B.K. Maheshwari and N. Karwa, Experimental study of heat transfer enhancement in an asymmetrically heated rectangular duct with perforated baffles, *Int. Commun. Heat Mass Transfer* **32** (2005), pp. 275-284.

[24] C.-W. Lin, Experimental study of thermal behaviors in a rectangular channel with baffle of pores, *Int. Commun. Heat Mass Transfer* **33** (2006), pp. 985-992.

[25] I. Kurtbas, The effect of different inlet conditions of air in a rectangular channel on convection heat transfer: Turbulence flow, *Experimental Thermal and Fluid Science* **33** (2008), pp. 140–152.

[26] W.A. El-Askary and M. Nasr, Performance of a bend–diffuser system: Experimental and numerical studies, Computers & Fluids **38** (2009) 160–170.

[27] M.A. Leschziner and W. Rodi, Calculation of annular and twin parallel jets sing various discretization schemes and turbulence-model variations, ASME J. Fluids Eng. **103**(1981), pp. 352-360.

[28] Z. Han and R.D. Reitz, Turbulence modeling of internal combustion engine using RNG k-ε model, Combust. Sci and Tech. **106** (1995), pp. 267-295.

[29] B. E. Launder and D. B. Spalding, The numerical computation of turbulent flows, Computer Methods in Applied Mechanics and Engineering, **3** (1974), pp. 269-289.

[30] S. V. Patankar, Numerical heat transfer and fluid flow, McGraw-Hill, New York, U.S.A., 1983.

8. NOMENCLATURE

c_1, c_2 , c_μ,	empirical constants of the k-ε model	
Cp	pressure coefficient	$(\overline{p}/0.5\,\rho U_{in}^2)$
d	channel hydraulic parameter	cm
H	channel height	cm
k	dimensionless turbulent kinetic energy $=\overline{k}/U_{in}^2$	
$\overline{k}$	turbulent kinetic energy	J/kg
p	dimensionless pressure	$(\overline{p}/0.5\,\rho U_{in}^2)$
$\overline{p}$	static pressure	N/m^2
Re	Reynolds number	$(Re=\rho U_{in} d/\mu)$
Re_t	turbulent Reynolds number	$(Re_t=\rho U_{in} d/\mu_t)$
u	Dimensionless x-component of local mean velocity	$(u=\overline{u}/U_{in})$
$\overline{u}$	x- component of local mean velocity	
U_{in}	average velocity of channel inlet m/sec	
v	dimensionless y- component of local mean velocity	$(v=\overline{v}/U_{in})$
$\overline{v}$	vertical component of local mean velocity m/sec	
x, y	cartesian coordinates	

Greeks

ε	Dimensionles dissipation rate of $\overline{k}$ $(\varepsilon=\overline{\varepsilon}\,d/U_{in}^3)$	
$\overline{\varepsilon}$	dissipation rate of $\overline{k}$	J/kg.sec
η_0	parameter in RNG k- ε model	
ν	kinematic viscosity	kg/m.sec
ρ	density	kg/m^3
σ_ε	model constant	
σ_κ	model constant	

Subscripts

c	curvature
in	Inlet
t	indices for turbulent
tot	total